A thylakoid biogenesis BtpA protein is required for the initial step of tetrapyrrole biosynthesis in cyanobacteria

Petra Skotnicová[1,2] (iD), Amit Srivastava[1,3] (iD), Divya Aggarwal[1,2] (iD), Jana Talbot[1,4] (iD), Iva Karlínová[5] (iD), Martin Moos[5] (iD), Jan Mareš[1,5] (iD), Lenka Bučinská[1] (iD), Peter Koník[1,2] (iD), Petr Šimek[5] (iD), Martin Tichý[1] (iD) and Roman Sobotka[1,2] (iD)

[1]Institute of Microbiology of the Czech Academy of Sciences, Centre Algatech, Třeboň, 379 01, Czech Republic; [2]Faculty of Science, University of South Bohemia, České Budějovice, 370 05, Czech Republic; [3]Department of Biological and Environmental Science, Nanoscience Centre, University of Jyväskylä, Jyväskylä, 40014, Finland; [4]Wicking Dementia Research and Education Centre, University of Tasmania, Hobart, Tas., 7005, Australia; [5]Biology Centre of the Czech Academy of Sciences, České Budějovice, 370 05, Czech Republic

Summary

• Biogenesis of the photosynthetic apparatus requires complicated molecular machinery, individual components of which are either poorly characterized or unknown. The BtpA protein has been described as a factor required for the stability of photosystem I (PSI) in cyanobacteria; however, how the BtpA stabilized PSI remains unexplained.

• To clarify the role of BtpA, we constructed and characterized the btpA-null mutant ($\Delta btpA$) in the cyanobacterium Synechocystis sp. PCC 6803. The mutant contained only c. 1% of chlorophyll and nearly no thylakoid membranes. However, this strain, growing only in the presence of glucose, was genetically unstable and readily generated suppressor mutations that restore the photoautotrophy.

• Two suppressor mutations were mapped into the hemA gene encoding glutamyl-tRNA reductase (GluTR) – the first enzyme of tetrapyrrole biosynthesis. Indeed, the GluTR was not detectable in the $\Delta btpA$ mutant and the suppressor mutations restored biosynthesis of tetrapyrroles and photoautotrophy by increased GluTR expression or by improved GluTR stability/processivity. We further demonstrated that GluTR associates with a large BtpA oligomer and that BtpA is required for the stability of GluTR.

• Our results show that the BtpA protein is involved in the biogenesis of photosystems at the level of regulation of tetrapyrrole biosynthesis.

Introduction

Oxygenic photosynthesis requires complicated molecular machinery embedded in a specialized membrane system and composed of many individual proteins, cofactors, and lipids. The function and structure of this apparatus, which is mostly conserved in cyanobacteria, algae, and plants, have been described in great detail; however, how photosynthetic complexes are built and maintained in the cell remains poorly understood. This especially applies to photosystem I (PSI), complex, as the biogenesis of photosystem II (PSII) has attracted much more research attention in recent years (Komenda & Sobotka, 2019).

When compared to > 20 auxiliary protein factors known to participate in PSII biogenesis (Heinz et al., 2016), the list is much shorter for factors involved in the assembly/maintaining of PSI complexes and many of them are specific to eukaryotic phototrophs (Roose et al., 2014; Shen et al., 2017; Nellaepalli et al., 2018). The BtpA protein (biogenesis of thylakoid proteins A; Bartsevich & Pakrasi, 1997) is so far the only reported PSI biogenesis factor that is not present in plants and algae but is

ubiquitous in cyanobacteria (with the exception of marine pico-cyanobacteria with highly reduced genomes; Mareš et al., 2019). Initially, a Synechocystis sp. PCC 6803 (hereafter Synechocystis) strain harboring a missense mutation in the btpA gene has been identified by screening of photosynthesis-deficient strains; the mutant suffered from depletion in PSI complexes while the PSII level appeared unaffected (Bartsevich & Pakrasi, 1997). Later, prepared btpA deletion mutant exhibited a significantly reduced chlorophyll (Chl) content in addition to the reduced level of the majority of PSI subunits. Also in the btpA deletion mutant, the PSII-mediated oxygen evolution was similar to wild-type (WT; Zak & Pakrasi, 2000). Interestingly, cyanobacterial BtpA belongs to a BtpA/SgcQ family of proteins with unknown function, which are dispersedly present in many bacterial, archeal, and eukaryotic species. However, the ubiquity of the ancient BtpA protein in cyanobacteria indicates that it has evolved to play some specific important role in this phylum.

Here, we prepared and characterized a new Synechocystis btpA-null mutant ($\Delta btpA$). This strain lacked both photosystems and thylakoid membranes and showed an extremely poor phenotype.

We found that in the absence of BtpA, glutamyl-tRNA reductase (GluTR) – the first enzyme in the tetrapyrrole pathway, did not accumulate in cells but the tetrapyrrole biosynthesis was restored by suppressor mutations stabilizing the GluTR enzyme. The BtpA was identified as a component of a protein assembly further consisting of GluTR, bifunctional glutamate/ornithine acetyltransferase enzyme (ArgJ), and an uncharacterized Slr1565-Slr1098 heterodimer (Morimoto *et al.*, 2002). We conclude that the thylakoid biogenesis protein BtpA is crucial for the post-translational regulation of GluTR in cyanobacteria.

Materials and Methods

Construction and cultivation of *Synechocystis* and *E. coli* strains

All *Synechocystis* strains used in this study (see Supporting Information Tables S1, S2 for a list of strains and primers) were derived from the glucose-tolerant, nonmotile GT-P sub-strain (Tichý *et al.*, 2016). Unless stated otherwise, strains were grown photoautotrophically in a rotary shaker under 40 µmol photons $m^{-2} s^{-1}$ (NL) and 28°C in liquid BG11 medium. For the preparation of the $\Delta btpA$ mutant, the DNA was isolated from the original $\Delta btpA$ strain (Zak & Pakrasi, 2000) obtained from Prof. Himadri Pakrasi (Washington University). The mutated locus was amplified by PCR and transformed into WT cells. The DNA construct for the replacement of *btpA* gene with an erythromycin resistance cassette was prepared using the megaprimer PCR-based mutagenesis approach (Lee *et al.*, 2004). All strains expressing N-terminally FLAG-tagged proteins were constructed using the pPD-*N*FLAG vector (Hollingshead *et al.*, 2012). This vector consists of native *psbAII* promoter for the expression of a cloned gene, a kanamycin resistance cassette for selection, and flanking sequences for homologous recombination in place of the *psbAII* gene. A similar DNA construct for the expression of N-terminally FLAG-tagged BtpA (f.BtpA), which contains erythromycin resistance, was chemically synthesized by Genscript (Piscataway, NJ, USA). *Synechocystis* transformants were selected on BG11 agar plates with increasing levels of the corresponding antibiotics. Complete segregation of the deletion strains was confirmed by PCR. $\Delta btpA$ strain was grown under 5 µmol photons $m^{-2} s^{-1}$ in BG11 medium supplemented with 5 mM glucose. For the f.BtpA, f.GluTR, and control pulldowns, the respective strains were grown photoautotrophically in 4 l of media in air-bubbled cylinders to an OD_{750nm} of 0.5–0.7. The *sgcQ* deletion mutant (*sgcQ769*(del)::kan) and the parent *E. coli* K12 strain were obtained from The Coli Genetic Stock Center (CGSC) at Yale University (Baba *et al.*, 2006). The cells were grown in LB media at 37°C and 180 rpm until exponential phase ($OD_{600nm} = 0.5$) and were flash-frozen in liquid N until further use.

Genetic mapping of suppressor mutants

The DNA for genomic sequencing of the suppressor mutants was isolated as described by Ermakova-Gerdes & Vermaas (1999), with slight modifications. Briefly, the cells were washed with saturated NaI solution and lysed by lysozyme and SDS. The lysate was treated with proteinase K, extracted with phenol, phenol/chloroform, and chloroform, and treated with RNase. The DNA was precipitated by sodium acetate and ethanol, briefly air-dried, and resuspended in water. The sequencing was performed commercially. One hundred base paired-end sequencing was performed on an Illumina HiSeq 2000 system. Raw paired reads were mapped to the GT-Kazusa sequence using CLC Genomics Workbench software (https://www.qiagenbioinformatics.com). Only variants with a higher than 50% frequency were considered.

Purification of protein complexes

Harvested cells were washed and resuspended in a buffer containing 20 mM Hepes pH 8, 20% glycerol, 150 mM NaCl, 1 mM EDTA, and then broken by glass beads. Complete Protease Inhibitor (Roche) was added to the buffer before breaking the cells. Membranes were pelleted by centrifugation (55 000 *g*, 20 min, 4°C) and resuspended in an excess of the buffer, and the centrifugation step was repeated. In more detail, the breaking procedure is described by Koskela *et al.* (2020). Anti-FLAG-M2 agarose resin (Sigma) was used for selective isolation of FLAG-tagged proteins. The soluble fraction was loaded directly onto the column. For the isolation of tagged protein from membrane fraction, the membranes were resuspended in the respective buffer and solubilized for 1 h at 10°C with 1.5% *n*-Dodecyl-β-D-maltoside (DDM; Enzo Life Sciences, Farmingsdale, NY, USA). After centrifugation (55 000 *g*, 20 min, 4°C), the pulldown assay was performed essentially as described in Koskela *et al.* (2020) using the Hepes buffer described above.

Electrophoresis and immunoblotting

For native electrophoresis, solubilized membrane proteins or isolated complexes were separated on 4–14% clear-native gel (CN-PAGE) or 4–14% blue-native gel (BN-PAGE) in the first dimension. As the Chl level of $\Delta btpA$ is extremely low, sets of samples, which included the *btpA* deletion mutant, were loaded according to the heme-*b* determined by high-performance liquid chromatography (HPLC; see later). To resolve individual components of protein complexes, the gel strip from the BN- or CN-PAGE was first incubated in 2% SDS and 1% dithiothreitol for 30 min at room temperature, and then, the proteins were separated along the second dimension by SDS-PAGE in a denaturing 12–20% polyacrylamide gel containing 7 M urea (Dobáková *et al.*, 2009). The protein composition of purified complexes was analyzed in the first dimension by SDS-PAGE of the same composition. Proteins separated by SDS-PAGE were stained with Coomassie brilliant blue or SYPRO Orange afterward. Mass spectrometry analysis of stained protein bands/spots from the SDS-PAGE gels was accomplished essentially as described by Bučinská *et al.* (2018). For detection by a specific antibody, proteins were transferred from the SDS gel to a polyvinylidene difluoride membrane (Immobilon-P; Merck Millipore, Darmstadt, Germany). This membrane was incubated with a respective primary antibody overnight at 10°C and then for 1 h at room temperature with a secondary antibody conjugated with

horseradish peroxidase (Sigma). The antibody specific to GluTR protein was raised in rabbit against recombinant GST-tagged *Synechocystis* GluTR protein; BtpA antibody (Zak *et al.*, 1999) was provided by Prof. Himadri Pakrashi (Washington University). Antibody raised in rabbit against the recombinant glutamyl-tRNA synthetase from *Tolypothrix* 7601 was provided by Prof. Ignacio Luque (University of Sevilla). D1 and PsaF antibodies were raised in rabbit against a synthetic peptide corresponding to amino acids 59–76 and 50–61 of *Synechocystis* D1 and PsaF proteins, respectively. Mg-protoporphyrin IX methyl ester cyclase and PetA antibodies were purchased from Agrisera (Sweden) and anti-FLAG from Abgent (catalog no. AP1013A). Antibodies against *Synechocystis* Mg-protoporphyrin IX methyltransferase and ferrochelatase were prepared in rabbits using full-length recombinant proteins. The dilution of used antibodies: GluTR (1 : 1000), BtpA (1 : 2000), glutamyl-tRNA synthetase (1 : 2000), D1 (1 : 5000), PsaF (1 : 2000), Mg-protoporphyrin IX methyl ester cyclase (1 : 3000), PetA (1 : 5000), FLAG (1 : 5000), Mg-protoporphyrin IX methyltransferase (1 : 3000), and ferrochelatase (1 : 5000).

Analysis of pigments and intermediates of tetrapyrrole pathway

Absorption spectra of whole cells were measured using a Shimadzu UV-3000 spectrophotometer (Kyoto, Japan). To determine Chl and carotenoid levels, pigments were extracted from cell pellets with 100% methanol and separated by HPLC essentially as described in Skotnicová *et al.* (2021). Heme-*b* was extracted by Acetone/0.2% HCl and immediately injected into a HPLC machine (Agilent Technologies, Santa Clara, CA, USA) and separated using the Nova-Pak C18 reverse-phase column (4 μm particle size, 3.9 × 75 mm; Waters, Wilmslow, UK) with 0.1% trifluoroacetic acid and acetonitrile/0.1% trifluoroacetic acid as solvents A and B, respectively. Extracted pigments were eluted with a linear gradient of solvent B (30–100% in 12 min) followed by 100% of B at a flow rate of 0.8 ml min^{-1} at 40°C. Heme-*b* was detected by diode array detector 1200 (Agilent) and identified by retention time and absorbance spectra according to standard of hemin (Sigma-Aldrich). Pyrrolic precursors of the heme/Chl biosynthetic pathway were quantified according to Pilný *et al.* (2015). To analyze UroP isomers, tetrapyrroles were extracted from cells according to Pilný *et al.* (2015) and separated on the Nova-Pak C18 column (4 μm particle size, 3.9 × 150 mm; Waters) with 1 M ammonium acetate pH 5.2 and 10% acetonitrile in methanol as solvents A and B, respectively. A linear gradient of solvent B (0–50% in 20 min) was followed by 100% of B for 15 min at a flow rate of 0.6 ml min^{-1} at 40°C. Coproporphyrin III and UroP III standards were obtained from Sigma, and UroP I standard was purchased from Frontier Scientific (USA).

Real-time quantitative PCR

The total RNA from exponentially grown (OD$_{750}$ = 0.4) cyanobacterial cells was extracted using the PGTX method of Pinto *et al.* (2009) and incubated at room temperature with Turbo DNase I (Ambion) to degrade the genomic DNA. The cDNA was prepared from 1 μg of RNA using 20 pmol of each primer, 2 μl of 10 mM dNTPs, 4 μl of reaction buffer (5× first strand buffer), 0.5 μl of RNAse inhibitor (40 U μl^{-1}), 0.2 μl SuperScript II Reverse Transcriptase (Invitrogen; 20 U μl^{-1}), and 10.5 μl of DEPC-treated water. The samples were incubated at 55°C (5 min), 85°C (5 min), and cooled at 10°C. Then, 5 μl of a 10-fold diluted cDNA sample was mixed with 5 μl of each primer (20 pmol) and 10 μl of iQ SYBR Green Supermix (Bio-Rad). The RT-qPCR was performed by Rotor-Gene RG-3000 (Corbett Research, Sydney, NSW, Australia), and the data were monitored by ROTOR-GENE 6 software. The RT-qPCR program was performed at 95°C for 10 min (initial hold), 95°C for 20 s, 55°C for 20 s, and 72°C for 30 s until 50 cycles. $2^{-\Delta\Delta C_T}$ was used to calculate relative quantities of transcripts using a housekeeping *rnpB* gene as a reference (Livak & Schmittgen, 2001). Each sample was tested in triplicate, and data were collected from at least three independent biological replicates and presented as mean ± SD.

Bioinformatic analysis

To investigate the distribution of target proteins (BtpA/SgcQ, ArgJ) encoded in (cyano)bacterial genomes, custom BLASTP (https://blast.ncbi.nlm.nih.gov) searches against relevant NCBI databases (*nr*, *wgs*) were performed, employing limits by Organism (taxid) and *e*-value cutoff 1e^{-10}, using the respective proteins from *Synechocystis* (BtpA, ArgJ) and *E. coli* (SgcQ) as queries. BtpA/SgcQ homologs harvested by the BLAST searches were aligned using MAAFT v. 7 (Katoh & Standley, 2013).

Quantitative LC–MS/MS analysis of 5-ALA

Samples, prepared as described in Methods S1, were subjected to LC–MS/MS, which was performed on an HPLC 1290 LC Infinity II coupled to a triple quadrupole mass spectrometer 6495B (Agilent Technologies). 5-ALA was separated on a 150 mm × 2.1 mm i.d., 2.6 μm, Kinetex (Phenomenex, Torrance, CA, USA) with a mobile phase flow rate of 200 μl min^{-1}, injection volume of 2 μl, column temperature of 35°C, and autosampler temperature of 10°C; see Methods S1 for details. Data were acquired using MASSHUNTER Workstation v.10.1 and processed using MASSHUNTER Quantitative Analysis v.9.0. The multiple reaction monitoring transitions are summarized in Table S3.

Protein mass spectrometry

For the preparation of samples for protein MS, see Methods S2. LC–MS/MS measurement was performed using NanoAcquity UPLC coupled online to the ESI Q-Tof Premier mass spectrometer (the instrument, columns, and software were from Waters). Peptides were separated by reverse-phase UPLC on the BEH300 C18 analytical column (75 mm i.d.; 150 mm length, particle size 1.7 mm) at 0.4 μl min^{-1} flow rate by a linearly increasing ratio of water : acetonitrile from 3% (v/v) to 40% during 30 min. Both mobile phases contained 0.1% (v/v) formic acid. Peptides eluted from the column flowed directly into the

electrospray ionization source. Data processing is described in Methods S2.

Electron microscopy

Pelleted cells were loaded and frozen in specimen carriers by EM PACT2 (Leica) high-pressure freezer and transferred into 2 ml cryovials with freeze-substitution medium under liquid N. Samples were processed as described in Methods S3. Ultra-thin sections (50–70 nm) were cut using UCT ultramicrotome (Leica) and collected on mesh copper grids (EMS) with the formvar coating. Sections were stained with 1% aqueous uranyl acetate for 10 min and with Sato's lead citrate for 3 min (Hanaichi et al., 1986). Images were acquired using a transmission electron microscope Jeol 1010 operated at 80 kV equipped with a Mega-View III camera (SIS).

Results

ΔbtpA strain lacks photosynthetic machinery

To clarify the role of the BtpA protein in cyanobacteria, we prepared a new Synechocystis ΔbtpA strain using our standard laboratory GT-P sub-strain (Tichý et al., 2016) and the identical construct described in Zak & Pakrasi (2000). Interestingly, the fully segregated ΔbtpA mutant exhibited a very pale-yellow color (Fig. 1a) and grew slowly even in the presence of glucose. Whole-cell absorption spectra showed a significantly reduced level of phycobiliproteins and no detectable Chl absorbance (Fig. 1a). A detailed pigment analysis revealed the presence of only c. 1% of Chl in the ΔbtpA mutant when compared to WT grown under the same conditions. The total carotenoid content was less affected; however, the level of β-carotene, a cofactor of photosystems, was drastically reduced (Fig. 1b). On the contrary, the level of heme-b in the mutant cells was lowered only to half of the level in WT (Fig. 1c). To verify that this severe phenotype is caused solely by the deletion of the btpA gene, the ΔbtpA strain was complemented with the ectopically expressed f.btpA gene coding for the BtpA fused with 3×FLAG-tagged at the N-terminus (f.BtpA; see Table S1 for a list of strains). Indeed, the level of pigments in the resulting $f.btpA^+/\Delta btpA$ strain was restored (Fig. 1a) and its photoautotrophic growth was comparable to WT (Fig. S1a).

The content of photosynthetic membrane protein complexes was further assessed by 2D clear-native/SDS electrophoresis (CN/SDS-PAGE). Although we typically calculate the amount of loaded membrane proteins according to the concentration of Chl, the loading of samples which included Chl-less ΔbtpA was calculated according to the content of heme-b (Fig. 2a, see Materials and Methods section for details). Separation of the gel strip from the first (native) dimension on SDS-PAGE was followed by SYPRO Orange stain. The result showed a dramatic decrease in the total content of membrane proteins in the mutant cells; nonetheless, levels of ATP synthase and NDH complexes remained comparable to WT (Fig. 2a). We then blotted proteins from the stained gel onto the polyvinylidene-fluoride membrane and probed the membrane with antibodies against PSI, PSII, and $b_6 f$ subunits (Fig. 2a). Similar to ATP synthase, the cytochrome $b_6 f$ was still relatively abundant in the mutant but both photosystems were almost completely lost. Interestingly, the partially matured intermediate of PSII core subunit D1 (iD1) can be detected in ΔbtpA, which suggests that the synthesis of D1 precursor does not require Chl (Fig. 2a). The drastic depletion in photosynthetic complexes was accompanied by changes in cell ultrastructure. As shown in Figs 2(b) and S2, ΔbtpA cells still contain a few short membrane fragments inside the cytoplasm but no organized network of thylakoid membrane sheets.

The photoautotrophy of the ΔbtpA is restored by mutations in the hemA gene

The phenotype of the ΔbtpA strain was not stable and the formation of fast-growing green ΔbtpA colonies (suppressor mutants) occurred frequently even on glucose-supplemented plates grown under low light (Fig. S1b). For further analysis, we selected two suppressor mutants (btpA-s1 and btpA-s2) that grew comparable to WT even under high-light stress and exhibited comparable pigmentation (Fig. 3a). We sequenced the genomes of btpA-s1 and btpA-s2 and identified a single suppressor mutation in each strain. Interestingly, both mutations are linked to the hemA gene coding for the GluTR enzyme that catalyzes the first enzymatic step of the tetrapyrrole pathway. Specifically, in the btpA-s1 strain, the mutation was mapped in −10 element of the hemA promoter, whereas the btpA-s2 strain harbors a point mutation in the hemA gene changing valine to leucine at the position 352 in GluTR (Fig. 3b). According to the predicted structure of the Synechocystis GluTR, the V352L mutation is physically distant from the catalytic center of the enzyme but it could distort the characteristic V-shape of the GluTR dimer (Fig. S3).

Analysis of suppressor strains signalized that the BtpA protein is functionally connected to the GluTR enzyme (tetrapyrrole pathway). We first checked the colocalization of both proteins in WT cells using immunoblotting and found that both GluTR and BtpA are mostly soluble proteins, just c. 25% of their total content can be detected in the membrane fraction (Fig. S4a). Then we prepared soluble and membrane protein fractions also from ΔbtpA and suppressor strains, and analyzed the level of GluTR. Importantly, this essential enzyme was undetectable in ΔbtpA but its level was partially restored by suppressor mutations (Fig. 3c). On the contrary, the level of glutamyl-tRNA synthetase providing glutamyl-tRNA for GluTR, but also for proteosynthesis, was unaffected in ΔbtpA. In addition, the content of heme-producing ferrochelatase enzyme was not lowered in the mutant as well as that of Mg-protoporphyrin IX methyltransferase, an enzyme specific to the Chl biosynthetic pathway.

The btpA-s1 suppressor mutation in the TATA box of hemA (Fig. 3b) indicated that the altered (enhanced) expression of hemA is sufficient to restore Chl biosynthesis and consequently, the accumulation of photosynthetic apparatus in ΔbtpA. This assumption was supported by 3.6× higher level of hemA mRNA
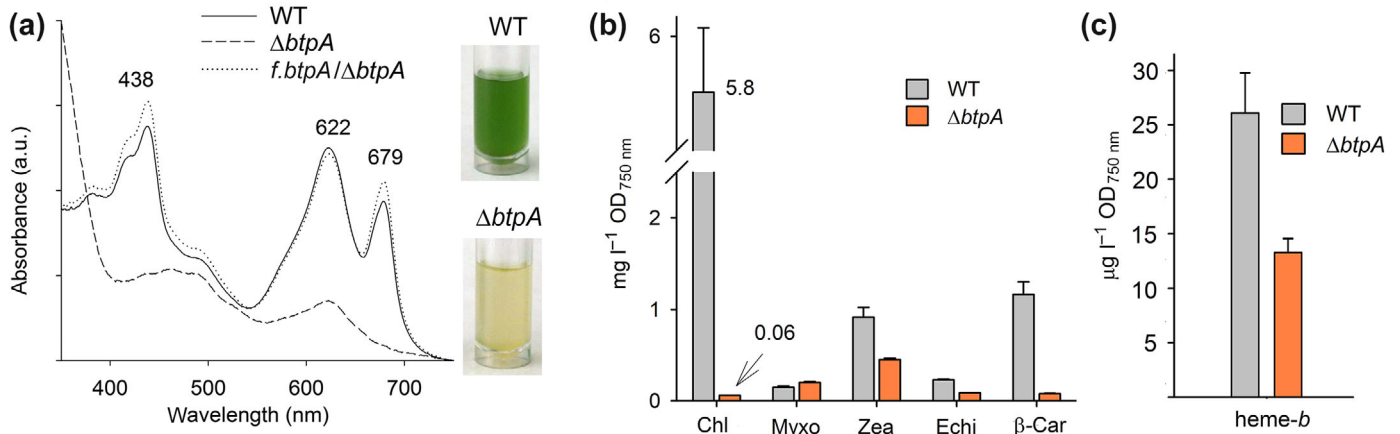
Fig. 1 Elimination of *btpA* gene drastically reduces chlorophyll level. (a) Whole-cell absorption spectra of wild-type (WT), *btpA*-null mutant (Δ*btpA)*, and *f.btpA*[+]/Δ*btpA* strains grown at 5 μmol of photons m[−2] s^{−1} (low light – LL) in the medium supplemented with 5 mM glucose; Chl is represented by peak at 679 nm and phycobiliproteins by peak at 622 nm. Spectra were normalized to light scattering at 750 nm. The content of photosynthetic pigments is fully restored in Δ*btpA* mutant ectopically expressing FLAG-tagged BtpA (f.BtpA) protein. The color of cell cultures at a similar optical density is also shown. (b) Content of pigments in WT and Δ*btpA* normalized to scattering at 750 nm. Pigments were extracted with methanol and quantified by high-performance liquid chromatography (HPLC); the error bars indicate the SD from the mean of biological triplicates. Echi, echinenone; Myxo, myxoxanthophyll; Zea, zeaxanthin; β-Car, β-carotene. (c) Heme-*b* was extracted by acetone/HCl from the same cultures as (b) and its concentration was determined by HPLC method.
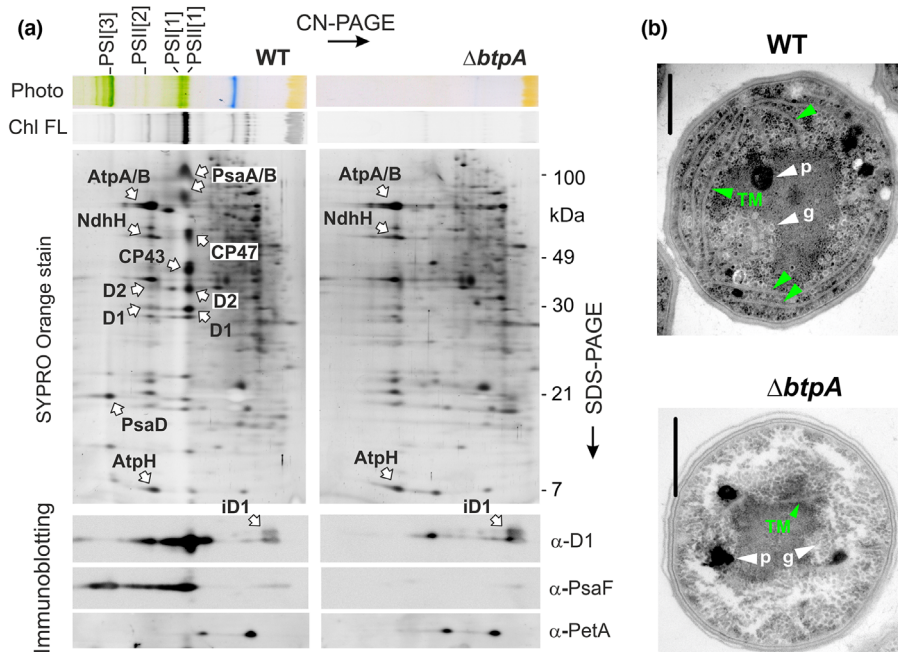

Fig. 2 The *btpA*-null mutant (Δ*btpA*) strain is devoid of both photosystems and thylakoid membranes. (a) The content of membrane protein complexes in wild-type (WT) and Δ*btpA* was analyzed by CN-PAGE followed by immunoblotting. The number of membrane proteins loaded for WT sample corresponded to 0.06 μg of heme-*b* while for Δ*btpA*, the amount was recalculated based on the heme-*b*/OD₇₅₀nm ratio in both strains (Fig. 1c). The gel was photographed (Photo) and scanned by LAS 4000 (Fuji) for chlorophyll fluorescence (Chl FL). The gel strips from CN-PAGE were further separated in a second dimension by SDS-PAGE and stained with SYPRO Orange. CP47, CP43, D1, and D2 subunits of photosystem II (PSII); PsaA/B and PsaD subunits of photosystem I (PSI), NDH, and ATP synthase (AtpA/B and AtpH), are marked according to Herranen *et al.* (2004). The gel was further blotted and the levels of D1, PsaF (PSI), and PetA (cytochrome *f*) were detected by a specific antibody. Designation of complexes: PSI[3] and PSI[1], trimeric and monomeric PSI; PSII[2] and PSII[1], dimeric and monomeric PSII. (b) Ultrastructure of WT and Δ*btpA* cells analyzed by transmission electron microscopy. Both strains were grown as described in Fig. 1. TM (green arrowheads), thylakoid membrane; g, glycogen granules; p, polyphosphate granules; bars, 500 nm. See Supporting Information Fig. S2 for more electron microscopic images.

in the *btpA*-s1 strain when compared to WT (Fig. 3d). To clarify the effect of *btpA* deletion on the initial steps of the tetrapyrrole pathway, we quantified the steady-state level of 5-aminolevulinic

acid (5-ALA) using LC–MS/MS analysis. The 5-ALA content in Δ*btpA* was only *c.* 18% of the level in WT cells grown under the same conditions (low light with glucose; Fig. 3e). On the
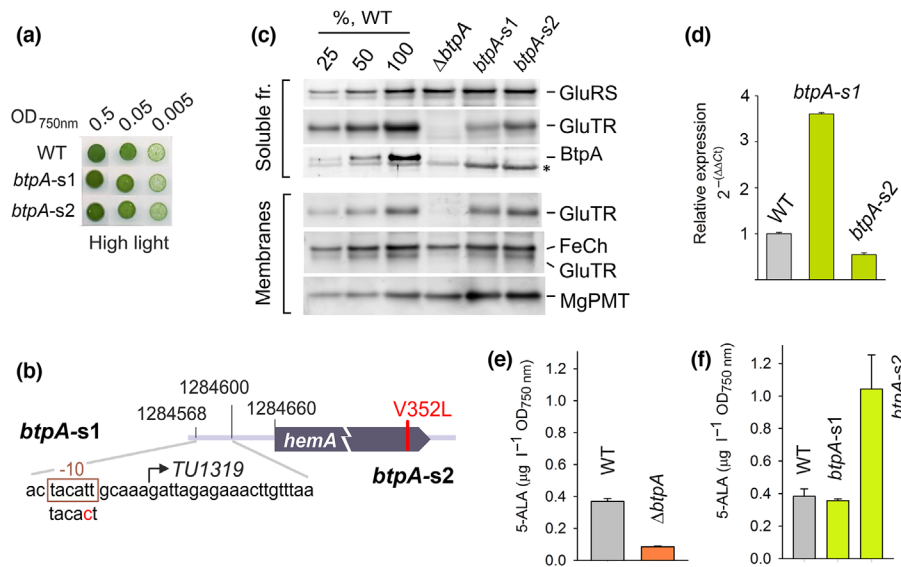
Fig. 3 Mutations suppressing the deletion of *btpA* are linked to *hemA* gene. (a) Photoautotrophic growth of two isolated *btpA*-null mutant (Δ*btpA*) revertant strains on agar plates under high-light conditions (300 μmol of photons m^{-2} s^{-1}). (b) An overview of mutations rescuing the photoautotrophic growth of the Δ*btpA* strain. The *btpA*-s1 strain contains a point nucleotide substitution in the −10 elements of the *hemA* gene coding for glutamyl-tRNA reductase (GluTR; transcription unit 1319; Kopf *et al.*, 2014), the mutation identified in the *btpA*-s2 strain is causing V352L amino acid substitution in the GluTR enzyme. (c) Immunodetection of enzymes in tetrapyrrole biosynthesis. All strains were grown mixotrophically under low light conditions and the isolated soluble (S) and membrane (M) fractions were separated by SDS electrophoresis and blotted; the load was calculated based on the heme-*b*/OD$_{750nm}$ ratio to correspond to the same number of cells (6 ng of heme-*b* for wild-type (WT)). Glutamyl-tRNA synthetase (GluRS), GluTR, BtpA, ferrochelatase (FeCh), and Mg-Protoporphyrin IX methyl transferase (MgPMT) were consecutively detected using specific antibodies. Star marks an unspecific cross-reaction of the α-BtpA antibody. (d) The level of *hemA* mRNA transcript in WT and Δ*btpA* revertant strains. All strains were grown photoautotrophically at 40 μmol photons m^{-2} s^{-1} (NL), the error bars indicate the SD from the mean of biological triplicates. (e) The cellular content of 5-aminolevulinic acid (5-ALA) in WT and Δ*btpA* strains grown at 5 μmol photons m^{-2} s^{-1} in the medium supplemented with 5 mM glucose. (f) The cellular content of 5-ALA in WT and Δ*btpA* revertant strains grown photoautotrophically at NL; the error bars indicate the SD from the mean of biological triplicates.

contrary, the 5-ALA content was fully restored in the *btpA*-s1 strain and significantly increased (2.7×) in *btpA*-s2 cells (Fig. 3f).

As a verification that the poor accumulation of GluTR accounts for the loss of Chl-binding complexes in Δ*btpA*, we transformed the mutant by a construct containing *f.hemA* gene coding for 3xFLAG-tagged GluTR (f.GluTR; see later) that was placed under a *psbAII* promoter. Strikingly, the resulting *f.hemA$^+$*/Δ*btpA* strain was capable to grow photoautotrophically (Fig. S1c) and exhibited a normal level of phycobiliproteins (Fig. 4a). The level of Chl complexes was lower than in WT but still much higher when compared to the original Δ*btpA* strain (Fig. 4a,b). It is notable that both f.GluTR and the native GluTR can be detected in *f.hemA$^+$*/Δ*btpA* cells but the level of each enzyme variant is low, no more than 25% level of the level of GluTR in WT (Fig. 4c). This would explain why the *f.hemA$^+$*/Δ*btpA* remains Chl deficient. In summary, these data suggested that the deletion of *btpA* gene mutant causes the instability of the GluTR enzyme but the poor phenotype can be at least partially complement by an additional copy of the (*f.*)*hemA* gene.

The tetrapyrrole pathway is upregulated in the *btpA*-s2 strain

Analysis of the tetrapyrrole pathway (Fig. 5a) in Δ*btpA* confirmed that the Chl branch is devoid of any detectable Chl

precursors except for monovinyl chlorophyllide (Fig. 5b). However, as has been shown earlier (Vavilin *et al.*, 2005), this metabolite can also originate from dephytylation of Chl and blocking the Chl biosynthetic pathway does not reduce the chlorophyllide level (Kopečná *et al.*, 2015). We expect that small amounts of Chl-binding proteins produced in Δ*btpA* undergo fast turnover, and the released Chls are dephytylated and re-phytylated many times. Since the lifetime of Chl molecules in *Synechocystis* is several days (Vavilin *et al.*, 2005), a significant pool of monovinyl chlorophyllide can accumulate in membranes even when the rate of *de novo* Chl formation is extremely low.

Upstream of the tetrapyrrole pathway, protoporphyrin IX (PP$_{IX}$) – the last common precursor for both heme and Chl biosynthesis, is still detectable in Δ*btpA* (*c.* 20% of WT level) but not coproporphyrinogen III, which is produced earlier in the pathway (Fig. 5b). We concluded that the amount of tetrapyrroles produced in Δ*btpA* is drastically reduced and the remaining available PP$_{IX}$ is channeled into the heme branch. As expected, the Chl biosynthesis was restored in *btpA*-s1 and *btpA*-s2 strains (Fig. 5c), even under photoautotrophic conditions. The entire tetrapyrrole pathway was, however, upregulated in the *btpA*-s2 as apparent from the increased accumulation of PP$_{IX}$ and coproporphyrin III by an order of magnitude (Fig. 5c). Moreover, *btpA*-s2 cells contained high levels of polar porphyrins, which were not present in WT (Fig. 5d). Because their absorption spectra and
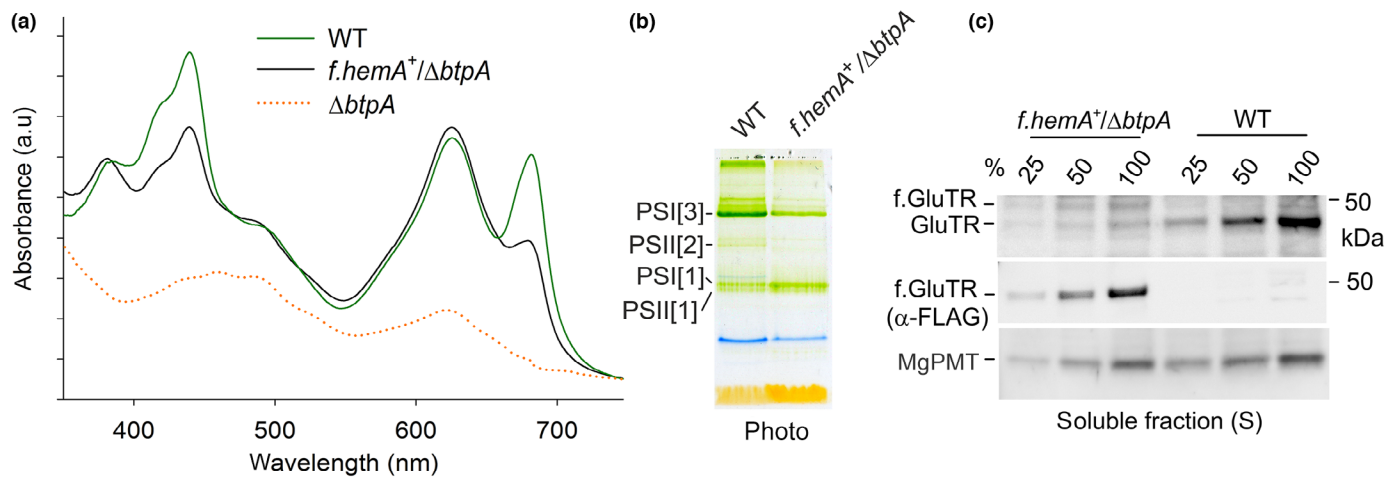
Fig. 4 Complementation of the *btpA*-null mutant (Δ*btpA*) mutation by the expression of *f.hemA* gene. (a) Whole-cell absorption spectra of wild-type (WT) and *f.hemA+*/Δ*btpA* cells grown photoautotrophically at 40 μmol photons m^{-2} s^{-1} (NL) together with Δ*btpA* grew heterotrophically under low light (5 μmol photons m^{-2} s^{-1}). (b) Solubilized membranes from WT and *f.hemA+*/Δ*btpA* strains grown photoautotrophically under NL were separated by CN-PAGE. For WT sample, membranes containing 5 μg of chlorophyll (Chl) were loaded, for *f.hemA+*/Δ*btpA* the amount was recalculated based on the Chl/OD$_{750nm}$ ratio in both strains. Designation of complexes: PSI[3] and PSI[1], trimeric and monomeric PSI; PSII[2] and PSII[1], dimeric and monomeric PSII. (c) Immunodetection of FLAG-tagged glutamyl-tRNA reductase (f.GluTR), nontagged GluTR, and Mg-protoporphyrin IX methyl transferase (MgPMT) enzymes in *f.hemA+*/Δ*btpA* cells grown photoautotrophically under NL.

HPLC retention time indicated uroporphyrin (UroPP) types of tetrapyrroles (Fig. S5), extracted pigments were analyzed by a HPLC method allowing to separate UroP isomers. We found that *btpA*-s2 cells accumulate UroP-III but also its UroP-I isomer (Fig. 5e) that origins from nonenzymatic cyclization of hydroxymethylbilane, the substrate of uroporphyrinogen III synthase (see Fig. 5a). Additional three UroP-like, but less polar tetrapyrroles, were also abundant in the *btpA*-s2 mutant (Figs 5e, S5; see the Discussion section).

As the transcript level of the *hemA-V352L* gene is lower than the level of *hemA* mRNA in WT (Fig. 3d), it is likely that the GluTR-V352L enzyme is more stable in the absence of BtpA. The mutated GluTR variant has to be highly active given the increased level of 5-ALA (Fig. 3f) and the accumulation of porphyrins in the *btpA*-s2 strain. In order to obtain an insight into a potential regulatory role of BtpA, we 'returned' the missing *btpA* gene into the *btpA*-s2 strain using the *f.btpA* construct described earlier. Interestingly, the expression of *f.btpA* restored the level of PP$_{IX}$ (Fig. 5c) and reduced the content of UroP porphyrins detected in *btpA*-s2 (Fig. 5d). Although the V352L mutation apparently disturbs the tetrapyrrole pathway, the mutated GluTR-V352L seems to be still under the control of BtpA.

GluTR, ArgJ, and the Slr1565-Slr1098 protein complex are co-purified with f.BtpA

The impaired GluTR accumulation in the Δ*btpA* strain could be explained by an interaction between GluTR and BtpA stabilizing the GluTR enzyme. As shown in Fig. 1(a) the f.BtpA protein expressed from the *psbAII* promoter is fully functional and complements the deletion of the *btpA* gene. We used the FLAG-epitope for the purification of f.BtpA protein from cellular soluble and membrane fractions. It is to be noted that the f.BtpA

protein was purified from cells containing also the native (nontagged) BtpA protein since the co-purification of tagged and nontagged variants could provide a hint about *in vivo* oligomerization of BtpA. The eluates obtained from *f.btpA* cells were separated on an SDS-PAGE, together with control elutions prepared from WT, and stained by Coomassie blue. A similar pattern of proteins was co-purified with f.BtpA from soluble and membrane fractions and most of the protein bands were identified by protein mass spectrometry (Fig. 6a; Table S4). The f.BtpA itself (bait) appeared in two bands with slightly different gel mobility, and GluTR represented another prominent band.

Another enzyme identified in the f.BtpA pulldown was bifunctional acetyltransferase ArgJ involved in arginine biosynthesis. As in many prokaryotes (Marc *et al.*, 2001), the *Synechocystis argJ* gene most likely encodes for an ArgJ precursor (43.3 kDa) processed by self-catalyzed cleavage into α and β chains (20 and 23.3 kDa). We detected two ArgJ proteins with masses *c.* 27 and *c.* 20 kDa (Fig. 6a), and our analysis of identified tryptic peptides agrees with the predicted ArgJ α and β chains (Fig. S6). In addition, f.BtpA was co-purified with an IscA homolog (Slr1565 or IscA2) and its protein partner named IaiH (Slr1098; Morimoto *et al.*, 2002; Fig. 6a).

The identical f.BtpA elution was separated on an SDS gel, blotted, and probed by α-GluTR and α-BtpA antibodies. This experiment confirmed that GluTR is specifically co-eluted with f.BtpA and is not present in the control elution. BtpA antibody identified also the nontagged BtpA in the elution, suggesting that the (f.)BtpA forms an oligomer or there are more copies of (f.)BtpA in the expected f.BtpA-GluTR complex (Fig. 6b).

In order to verify the interaction between BtpA and GluTR, we employed a *Synechocystis* strain possessing the *f.hemA* gene placed under a strong *psbAII* promoter. The produced f.GluTR protein possesses 3×FLAG-tag at its N-terminus and can
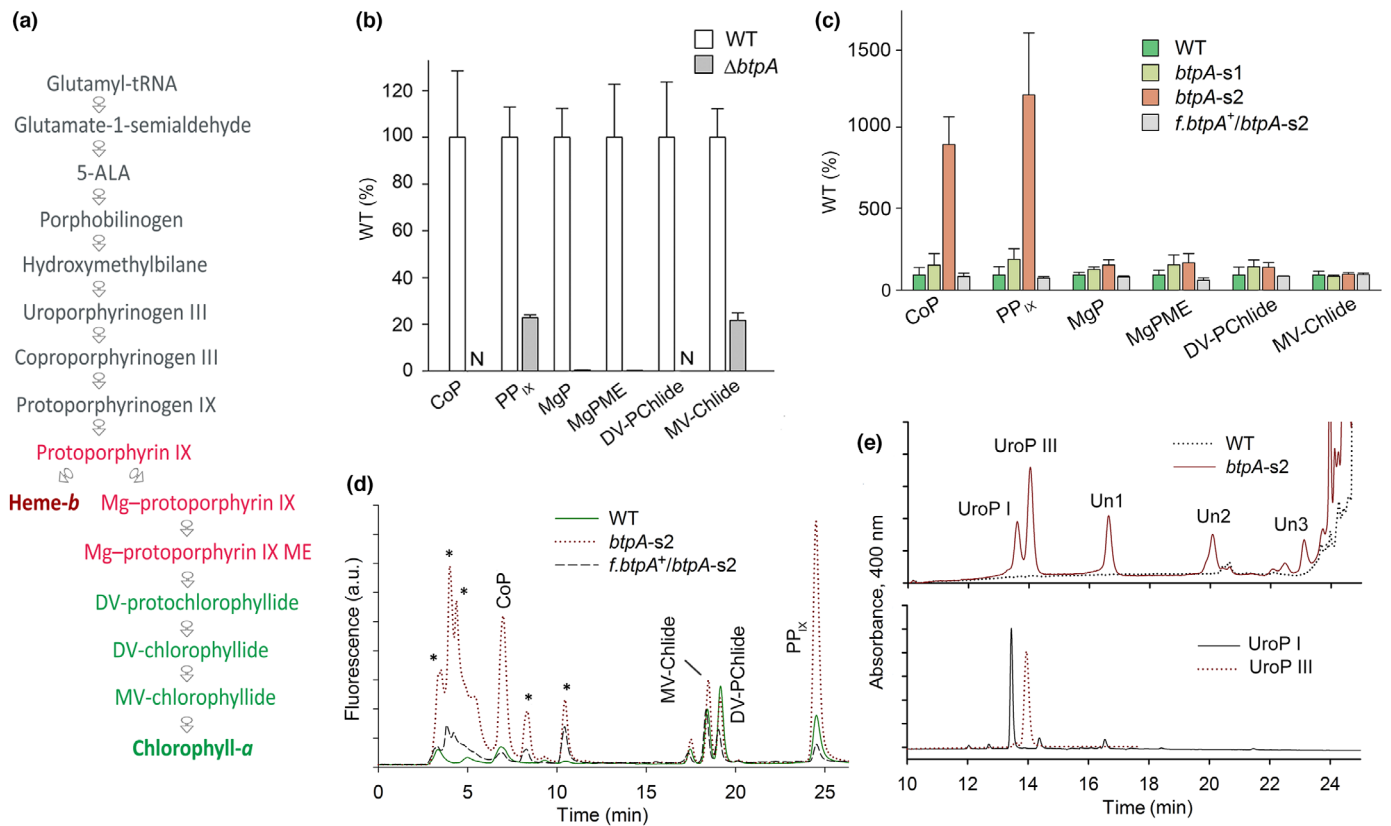
Fig. 5 Chlorophyll (Chl) biosynthetic pathway, abolished in the *btpA*-null mutant (Δ*btpA*), is restored in *btpA*-suppressor strains. (a) Biosynthetic pathway of heme and Chl in cyanobacteria. (b) Tetrapyrroles were extracted from 2 ml of cells with OD$_{750nm}$ = c. 0.4 grown mixotrophically under low light (5 μmol of photons m^{-2} s^{-1}). The obtained extract was analyzed by high-performance liquid chromatography (HPLC) equipped with two fluorescence detectors set on different excitation and emission wavelengths (Pilný *et al*., 2015). Coproporhyrinogen III (oxidized to coproporhyrin III – CoP) and protoporphyrin IX (PP$_{IX}$) are common precursors for both Chl and heme synthesis. The first committed intermediate of Chl pathway is Mg-protoporphyrin IX (MgP), which is consequently methylated (MgPME). The MgPME is converted into divinyl protochlorophyllide (DV-PChlide) and then into monovinyl chlorophyllide (MV-Chlide). Chl is finally made by attachment of phytol to the MV-Chlide. N = below a detection level. (c) Tetrapyrroles were extracted from 2 ml of cells with OD$_{750nm}$ = c. 0.4 grown photoautotrophically at 40 μmol photons m^{-2} s^{-1}. The level of precursors is shown as a ratio to the wild-type (WT) level and the error bars indicate the SD from the mean of biological triplicates. (d) Representative HPLC chromatograms of Chl precursor analysis (c) showing unknown polar porphyrins (marked by asterisks) that accumulate in *btpA*-s2 and partially also in *f.btpA⁺*/*btpA*-s2 strains. (e) Analysis of uroporphyrins (UroP) in WT and *btpA*-s2 strains. Extracted pigments were separated by HPLC and UroP I and III were detected by absorbance at 400 nm. Three unknown tetrapyrroles with absorbance spectra close to UroP are labelled Un1-3 (see Supporting Information Fig. S5).

functionally replace the native GluTR. The f.GluTR pulldowns were analyzed essentially as described for the f.BtpA. Remarkably, the spectrum of proteins co-purified with f.GluTR matched the f.BtpA isolation, including two forms of BtpA (Fig. 6a,b). The native (nontagged) GluTR was also co-isolated with f.GluTR, in particularly high amounts from the soluble fraction. To exclude that the GluTR, BtpA, ArgJ, or Slr1565 bind to 3×FLAG epitope, we isolated 3×FLAG-tagged geranylgeranyl reductase enzyme as another control (Koskela *et al*., 2020); however, these proteins were not detected on the stained gel and GluTR was not detectable even by antibodies (Fig. 6c,d).

GluTR is associated *in vivo* with a large BtpA oligomer

To obtain more details about the structural organization of the GluTR-BtpA assembly, we separated f.BtpA pulldown on the 2D blue-native/SDS electrophoresis, stained the obtained gel and identified the protein spots by mass spectrometry (Fig. 7a;

Table S4). Notably, the f.BtpA migrated on the gel as two large oligomers (c. 250 kDa and c. 500 kDa) and the same pattern shows also the nontagged BtpA co-purified with the f.BtpA bait. The co-isolated GluTR enzyme comigrated clearly with the (f.) BtpA oligomer, implying a stable physical interaction between these proteins. ArgJ enzyme and Slr1098-Slr1565 subcomplex probably dissociated during electrophoresis from other components of the complex (f.BtpA or GluTR). ArgJ (44 kDa) is apparently also an oligomer with a total mass c. 150 kDa, which would indicate a heterooctameric (α4β4), rather than heterotetrameric (α2β2) structure reported for bacterial ArgJ enzymes (de la Fuente *et al*., 2004).

To confirm that the observed BtpA oligomers are not just an artifact of protein isolation, we separated the total soluble fraction, prepared from the *f.btpA⁺* strain, by 2D blue-native/SDS electrophoresis. After blotting, the f.BtpA protein was immunodetected with anti-FLAG antibody. It revealed two large f.BtpA complexes with masses very similar to what we observed for the
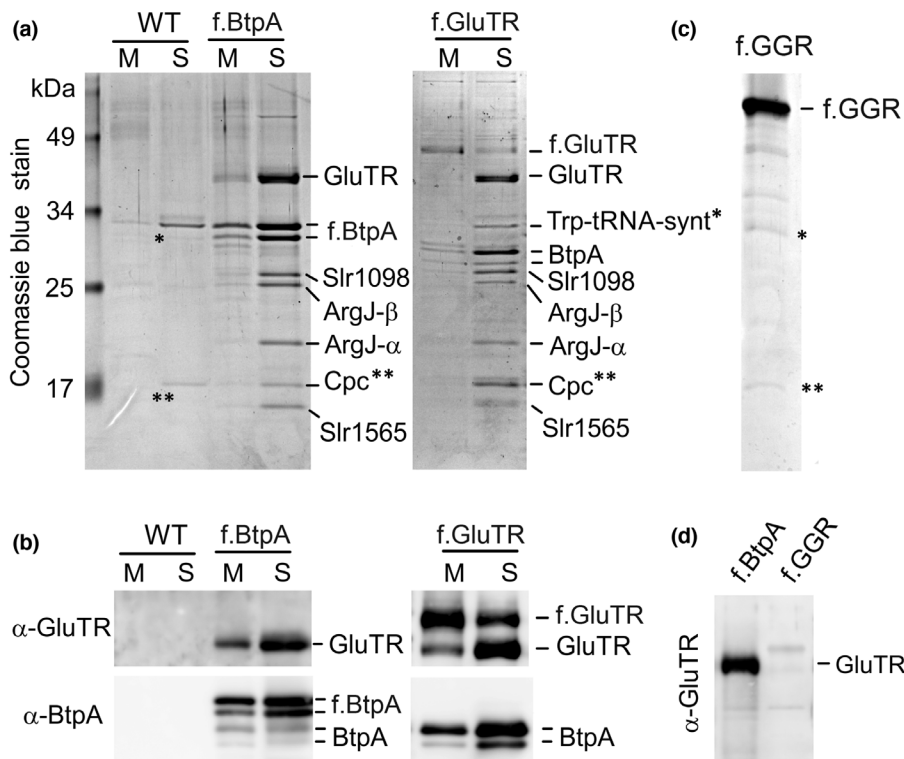
Fig. 6 Separation and MS analysis of FLAG-tagged BtpA (f.BtpA), f.GluTR, and f.GGR pulldowns. (a) f.BtpA and f.GluTR proteins were isolated using anti-Flag resin from soluble (S) and membrane (M) cellular fractions prepared from f.btpA⁺ and f.hemA⁺ strains. The obtained pulldowns (1/3 of the total volume) were separated by SDS-PAGE together with control eluates from wild-type (WT) cells and stained by Coomassie blue. Indicated proteins were identified by protein mass spectrometry (Supporting Information Table S4); Trp-tRNA-synt (*) and Cpc (**) – tryptophanyl-tRNA-synthetase and CpcA/B subunits of phycobilisomes are known unspecific interactors with the anti-FLAG resin (Knoppová *et al.*, 2014). (b) Other fractions (1/8) of identical pulldowns were separated by SDS-PAGE, blotted and probed by α-GluTR and α-BtpA antibodies. (c) SDS-PAGE of a control FLAG elution (one-third of the total volume) purified from the whole-cell extract of the f.chlP⁺ *Synechocystis* strain expressing FLAG-tagged geranylgeranyl reductase (f.GGR). (d) Immunoblotting showing the absence of GluTR in the f.GGR elution; f.BtpA elution from the soluble fraction served as a positive control.

purified f.BtpA (Fig. 7b) on the stained gel. Unfortunately, our anti-GluTR antibody did not detect the GluTR protein on 2D blots, which left open the question of how large is the cellular pool of GluTR associated with BtpA. Instead, we assessed by immunoblotting what fraction of the total soluble GluTR is co-isolated with f.BtpA in our pulldown assay. Fig. S4(b) shows that > 50% of the GluTR, loaded with other soluble proteins from the *f.btpA* strain on the anti-FLAG column, bound to the resin (Fig. S4b). As it is very likely that some complexes dissociated during cell fractionation and chromatography and not all f.BtpA bound the resin (Fig. S4b), we can conclude that the majority of cellular GluTR is in a protein complex with f.BtpA.

Post-translational regulation of the GluTR activity during nitrogen deprivation

In order to assess by what type of post-translational mechanism (degradation or/and inactivation) the GluTR-associated proteins control this enzyme, we monitored the level of Chl precursors and the level of GluTR during a short-term nitrogen (N) depletion. We have shown previously that the tetrapyrrole pathway in *Synechocystis* is completely switched off in N-deprived conditions (Chen *et al.*, 2021). The GluTR enzyme produces the rate-limiting precursor for all tetrapyrroles (Brzezowski *et al.*, 2015) and thus needs to be inactive during N deprivation. As shown in Fig. 8(a), already in 20 min after removing N from the growth medium, the content of most of metabolites in the tetrapyrroles pathway dropped down to a barely detectable level. Nonetheless, on the protein level, the GluTR appeared stable with no significant decrease in the soluble fraction in 1 h. Even after a long

(12 h) cultivation of cells without N, the GluTR level was still *c.* 25% of the level before treatment. Only a small amount of the total cellular GluTR was localized in the membrane fraction but even the membrane-bound GluTR appeared stable (Fig. 8b). This finding contrasted sharply with almost complete degradation of Mg-protoporphyrin IX methyl ester cyclase (AcsF), an enzyme producing protochlorophyllide, in 4 h (Fig. 8b). It appears therefore likely that the activity of GluTR is inhibited post-translationally almost immediately after the shortage of N while the degradation of GluTR comes later as a relatively slow response.

Discussion

The tetrapyrrole pathway needs to be well-regulated in virtually any type of organism since PP$_{IX}$ and other pyrrolic intermediates are highly phototoxic. Because the tetrapyrrole pathway is branched in oxygenic phototrophs and high quantities of end products (Chl, heme, bilins) are required for photosynthesis (Bryant *et al.*, 2020), a sophisticated controlling mechanism(s) must evolve in cyanobacteria balancing the pathway with other processes in the cell.

The GluTR enzyme, catalyzing the first committed step for the biosynthesis of all tetrapyrroles, is active as a homodimer (Fig. S3; Zhao *et al.*, 2014) and belongs to key regulatory targets of the pathway, particularly at the post-translational level (Brzezowski *et al.*, 2015; Wang & Grimm, 2021). In plants, GluTR has been found in a complex with FLU and GBP proteins (Czarnecki *et al.*, 2011) and the structure of the ternary GluTR-FLU-GBP complex has been solved (Fang *et al.*, 2016). The
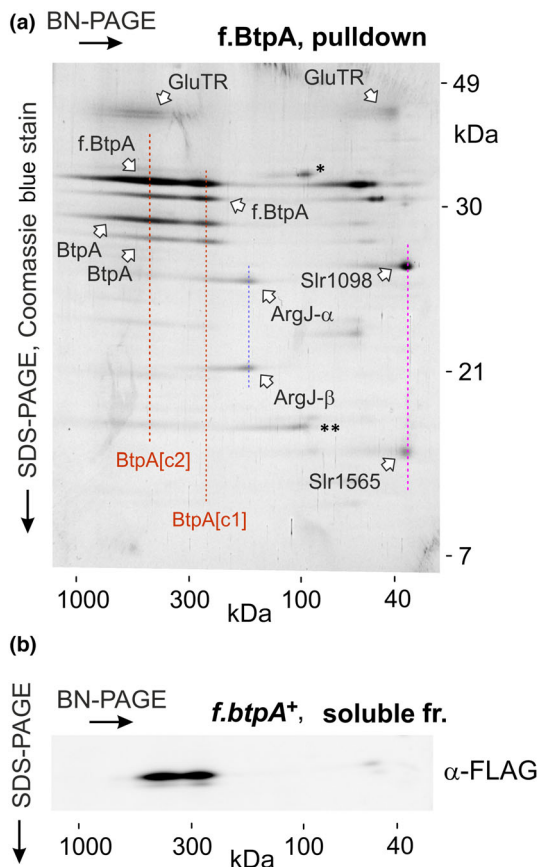
(a) BN-PAGE →

f.BtpA, pulldown

Fig. 7 2D BN/SDS-PAGE of the FLAG-tagged BtpA (f.BtpA) pulldown and detection of soluble f.BtpA complex on 2D blot. (a) f.BtpA protein was isolated using anti-FLAG resin from soluble fraction prepared from the *f.btpA+* strain. The obtained pulldown was separated first by blue-native (BN) gel and then in a second dimension by SDS-PAGE and stained with Coomassie blue. The obtained protein spots were analyzed by protein mass spectrometry (Supporting Information Table S4); * and ** – tryptophanyl-tRNA-synthetase and CpcA/B subunits of phycobilisomes, both unspecific interactors with the anti-FLAG resin (see Fig. 6a). Dashed lines indicate co-migrating proteins; BtpA[c1] and BtpA[c2] designate two putative BtpA oligomers. (b) Separation of total soluble proteins prepared from the *f.btpA+* strain on the 2D BN/SDS-PAGE. The gel was blotted on a polyvinylidene difluoride membrane and the f.BtpA protein was detected by anti-FLAG antibody.

membrane-bound FLU protein is essential for a feedback regulation that represses the GluTR activity if the level of Chl precursor protochlorophyllide over-accumulates, typically after a shift to darkness (Wang & Grimm, 2021). GBP is a heme-binding protein expected to dock GluTR to the membrane to partition a pool of the produced 5-ALA for the synthesis of heme. After binding of heme to GBP, the association of this protein with GluTR is weakened and the GBP-free GluTR is accessible to degradation by a Clp protease (Richter *et al.*, 2019). The soluble fraction of GluTR is further stabilized by cpSRP43, and according to the current model, this interaction coordinates the GluTR activity (Chl biosynthesis) with the biogenesis of light-harvesting complexes (Wang & Grimm, 2021).

Cyanobacteria do not use plant-type light-harvesting complexes. Instead, light is harvested by phycobilisomes containing

heme-based bilins as chromophores and serving also as an N reserve. Given further the fact that cyanobacteria can synthesize Chl in the dark, the post-translational regulation of GluTR in cyanobacteria can differ completely from that of plants. Indeed, cyanobacteria possess neither FLU nor GBP homologs. Although the formation of 5-ALA in cyanobacteria seems to be also controlled by a heme-feedback loop (Sobotka *et al.*, 2005, 2008), the BtpA probably does not bind heme as the purified recombinant BtpA is colorless (Schwabe *et al.*, 2003). We do not expect that the BtpA functionally mimics GBP although there seems to be a similar mode of post-translational control via conditional stability of GluTR during long-term N depletion. Similarly, a large excess of FLU protein in Arabidopsis mutant lines protects the GluTR against the proteolytic degradation (Hou *et al.*, 2021) but this effect might not be physiologically relevant. As widely expected, the primary role of FLU is to control the GluTR activity (not its stability), by sequestering the GluTR to a membrane-localized inactivation complex (Hou *et al.*, 2019). On the contrary, in *Synechocystis* depleted in N, the nonactive GluTR is not relocalized (Fig. 8b) and there is also no obvious difference in f.BtpA pulldowns purified from soluble and from membrane fractions (Fig. 6a). Zak *et al.* (1999) reported that by using buffer with 0.5 M sucrose, a large fraction of the *Synechocystis* BtpA protein can be localized in membranes. It is thus rather likely that the (active) BtpA-GluTR complex can weakly bound to the membrane, which also argues against analogy between the FLU-based mechanism in plants and the regulation of GluTR in cyanobacteria.

The Δ*btpA* mutant described here contains extremely reduced content of tetrapyrroles and our work clearly linked its phenotype to the GluTR enzyme. The original Δ*btpA* mutant (Zak & Pakrasi, 2000) was not able to grow photoautotrophically at low temperature and its transfer from optimal to low temperature led to degradation of core PsaA/B subunits of PSI (Zak & Pakrasi, 2000). The phenotype of our Δ*btpA* strain was much more pronounced, lacking both photosystems and thylakoid membranes. As the particular *btpA* mutation in both strains was identical, the observed difference in phenotypes may be explained by different genetic backgrounds of used WT strains. Significant phenotypic differences in *Synechocystis* 'WTs' have been already demonstrated (Tichý *et al.*, 2016). Another possibility is that the previously described Δ*btpA* strain (Zak & Pakrasi, 2000) possessed a suppressor mutation, taking into account the high frequency of their formation (Fig. S1b). Nonetheless, the impact of suppressor mutations in *Synechocystis* can be very complex (see e.g. Chen *et al.*, 2021), and resolving this discrepancy is thus hardly possible without knowing the genomic sequence of the original Δ*btpA* mutant.

BtpA forms large oligomers (Fig. 7a) and, as well as its bacterial homolog SgcQ, belongs to structural group of TIM (triosephosphate isomerase) barrel proteins (Fig. S7). Although TIM proteins are diverse, they are nearly always enzymes; *c.* 10% of all enzymes in nature belong to the TIM protein superfamily (Nagano *et al.*, 1999). In *E. coli*, *sgcQ* is a part of the *sgc* operon (*sgcXBCQAER*), which encodes a phosphotransferase system for the uptake of an unknown sugar (Curran *et al.*, 2017) and is
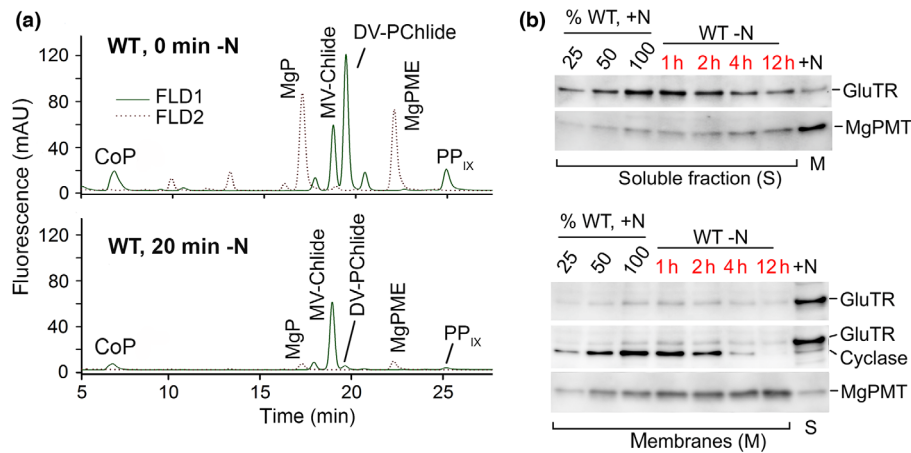
Fig. 8 Analysis of chlorophyll (Chl) precursors and glutamyl-tRNA reductase (GluTR) level in *Synechocystis* wild-type (WT) during nitrogen depletion. (a) Strains were grown photoautotrophically under 100 μmol of photons m^{-2} s^{-1} and subjected to nitrogen (N) starvation. Tetrapyrroles were extracted from 2 ml of cells with OD$_{750nm}$ = *c*. 0.4 before and after 20 min of N depletion. The obtained extract was analyzed by high-performance liquid chromatography (HPLC) equipped with two fluorescence detectors set on different excitation and emission wavelengths (Pilný *et al.*, 2015). CoP, Coproporhyrin III; DV-PChlide, divinyl protochlorophyllide; MgP, Mg-protoporphyrin IX; MgPME, Mg-protoporphyrin IX methyl ester; MV-Chlide, monovinyl chlorophyllide; PP$_{IX}$, protoporphyrin IX. (b) Immunodetection of selected *Synechocystis* Chl biosynthetic enzymes during N depletion; the isolated soluble (S) and membrane (M) fractions were separated by SDS electrophoresis and blotted, the load corresponded to the same number of cells (0.25 μg of Chl for WT). GluTR, Mg-protoporphyrin IX methyl ester cyclase (cyclase), and Mg-protoporphyrin IX methyl transferase (MgPMT) were consecutively detected using specific antibodies. To compare the level of each enzyme in the soluble and membrane fraction before N depletion, a sample of membrane proteins (+N; 100%) was included in the analysis of the soluble fraction and vice versa.

annotated as putative nucleoside triphosphatase (Keseler *et al.*, 2005). In contrast to *Synechocystis*, the *sgcQ* mutant of *E. coli* contained a normal level of PP$_{IX}$ (Fig. S8) and showed no obvious phenotype. Genomic context of BtpA in cyanobacteria is completely different and many Sgc proteins do not have clear cyanobacterial homologs. It is therefore possible that various proteins from the BtpA/SgcQ family have different functions. Apart from catalyzing various enzymatic reactions, they could serve solely a regulatory (structural) role, for example as a scaffold system for the GluTR regulatory complex in cyanobacteria. We are tempted to speculate that if the GluTR is inactive for a longer period (e.g. in N-deprived conditions; Fig. 8), it dissociates from BtpA and the released 'free' GluTR is targeted for proteolysis.

The elimination of BtpA would thus effectively mimic the dissociation of the complex, which explains the drastically reduced level of GluTR in Δ*btpA* (Fig. 3c). Notably, the GluTR can be stabilized by V352L mutation, which is probably changing the geometry of the GluTR homodimer to a more open Y-shape (Fig. S3). This seemingly subtle structural modification of GluTR has a great impact on the enzyme activity, which is manifested by almost three times higher steady-state level of 5-ALA (Fig. 3f) and by massive accumulation of PP$_{IX}$ (Fig. 5c). The fact that the mutated GluTR accumulates to a relatively high level (Fig. 3c) further implies the improved stability of the enzyme. The structural changes caused by the V352L substitution thus probably weakened the recognition of GluTR by a protease.

BtpA-s2 cells also contain high concentrations of UroP I and III together with unknown UroP derivatives (Fig. 5e, marked Un1-3). As indicated by a periodical HPLC mobility shift, these compounds might be hepta-, hexa-, and pentacarboxylic UroP (Figs 5e, S5). It is possible that uroporphyrinogen-I, formed due to an excess of hydroxymethylbilane, cannot be fully

decarboxylated by *Synechocystis* uroporphyrinogen decarboxylase or this enzyme is partially blocked by porphomethene (Phillips *et al.*, 2007). The expression of f.BtpA somehow suppresses the high activity of the mutated V352L GluTR and we could therefore speculate that the BtpA oligomer helps to connect various signals (protein factors) controlling the GluTR activity.

A component of the BtpA-GluTR complex is the bifunctional ArgJ enzyme catalyzing the synthesis of acetyl-glutamate, the starting metabolite of the arginine pathway. Acetyl-ornithine, produced later in the pathway, serves as the acetyl donor for the glutamate acetylation, which couples the first step of the pathway with the synthesis of ornithine. This cyclic type of arginine pathway is widely distributed in cyanobacteria as well as in algae and plants (Flores *et al.*, 2019). We searched for the presence of ArgA acetyltransferase, the enzyme specific for the linear-type of arginine pathway, in currently available cyanobacterial genomes using BLASTP; however, we got no single hit. It suggests that cyanobacteria use exclusively the bifunctional ArgJ enzyme. The arginine pathway plays a central role in maintaining N homeostasis as the surplus N is primarily used for the synthesis of this N-rich amino acid that can be further stockpiled in storage material, such as cyanophycin. Tightly controlled arginine biosynthesis/catabolism thus virtually always reflects the cellular N status and the first enzyme of this pathway (ArgJ) could indeed participate in the regulation of tetrapyrrole pathway (via interaction with GluTR-BtpA) during fluctuating N availability.

Deprivation in N blocks the tetrapyrrole pathway in *Synechocystis* in < 20 min (Fig. 8a) although the level of GluTR enzyme is reduced only slowly. The activity of this key enzyme thus must be quickly inhibited and we see as likely that the discovered interactions between GluTR-BtpA, ArgJ, and Slr1098-Slr1565 are implicated in this inhibition and generally in adjusting the

GluTR activity according to the actual cell homeostasis. Slr1565-Slr1098 is a heterodimer (Fig. 7a) containing a [2Fe-2S] cluster that is bound to Slr1565 (IscA2) and stabilized by Slr1098 (Morimoto *et al.*, 2003). It has been proposed that this [2Fe-2S] cluster acts as a molecular sensor of iron status (Balasubramanian *et al.*, 2006) or the redox state of cellular thiols (Morimoto *et al.*, 2003). It is not difficult to imagine the Slr1565-Slr1098 as a part of signaling cascade controlling the GluTR activity/stability during iron or redox disbalance. Altogether, our data show that the cyanobacterial BtpA protein is the part of a regulatory hub part directly inter-connecting the GluTR with different processes such as N and iron metabolism.

Competing interests

None declared.

Author contributions

PS, MT and RS designed the research. PS, AS, DA, JT, JM, LB, PK, MT, MM, IK and RS performed the research. PS, AS, PŠ, MT and R.S. analyzed the data. PS, MT and RS wrote the paper.

ORCID

Divya Aggarwal https://orcid.org/0000-0002-9648-2774
Lenka Bučinská https://orcid.org/0000-0002-4594-1600
Iva Karlínová https://orcid.org/0000-0002-7900-3794
Peter Koník https://orcid.org/0000-0001-8652-5323
Jan Mareš https://orcid.org/0000-0002-5745-7023
Martin Moos https://orcid.org/0000-0003-3930-3132
Petr Šimek https://orcid.org/0000-0003-2754-6372
Petra Skotnicová https://orcid.org/0000-0002-6077-0256
Roman Sobotka https://orcid.org/0000-0001-5909-3879
Amit Srivastava https://orcid.org/0000-0001-6541-5993
Jana Talbot https://orcid.org/0000-0003-2863-4139
Martin Tichý https://orcid.org/0000-0003-2814-1959

Data availability

The original contributions presented in the study are included in the article and the associated Supporting Information. The proteome datasets have been deposited in the MassIVE repository at https://massive.ucsd.edu, reference no. MSV000092431. Raw sequence data generated as part of this study are available from NCBI GenBank under BioProject PRJNA1024404.

References

Baba T, Ara T, Hasegawa M, Takai Y, Okumura Y, Baba M, Datsenko KA, Tomita M, Wanner BL, Mori H. 2006. Construction of *Escherichia coli* K-12 in-frame, single-gene knockout mutants: the Keio collection. *Molecular Systems Biology* **2**: 8.

Balasubramanian R, Shen G, Bryant DA, Golbeck JH. 2006. Regulatory roles for IscA and SufA in iron homeostasis and redox stress responses in the cyanobacterium *Synechococcus* sp. strain PCC 7002. *Journal of Bacteriology* **188**: 3182–3191.

Bartsevich VV, Pakrasi HB. 1997. Molecular identification of a novel protein that regulates biogenesis of photosystem I, a membrane protein complex. *Journal of Biological Chemistry* **272**: 6382–6387.

Bryant DA, Hunter CN, Warren MJ. 2020. Biosynthesis of the modified tetrapyrroles-the pigments of life. *Journal of Biological Chemistry* **295**: 6888–6925.

Brzezowski P, Richter AS, Grimm B. 2015. Regulation and function of tetrapyrrole biosynthesis in plants and algae. *Biochimica et Biophysica Acta-Bioenergetics* **1847**: 968–985.

Bučinská L, Kiss E, Koník P, Knoppová J, Komenda J, Sobotka R. 2018. The ribosome-bound protein Pam68 promotes insertion of chlorophyll into the CP47 subunit of photosystem II. *Plant Physiology* **176**: 2931–2942.

Chen GE, Hitchcock A, Mareš J, Gong Y, Tichý M, Pilný J, Kovářová L, Zdvihalová B, Xu J, Hunter CN *et al.* 2021. Evolution of Ycf54-independent chlorophyll biosynthesis in cyanobacteria. *Proceedings of the National Academy of Sciences, USA* **118**: e2024633118.

Curran TD, Abacha F, Hibberd SP, Rolfe MD, Lacey MM, Green J. 2017. Identification of new members of the *Escherichia coli* K-12 MG1655 SlyA regulon. *Microbiology* **163**: 400–409.

Czarnecki O, Hedtke B, Melzer M, Rothbart M, Richter A, Schroter Y, Pfannschmidt T, Grimm B. 2011. An Arabidopsis GluTR binding protein mediates spatial separation of 5-aminolevulinic acid synthesis in chloroplasts. *Plant Cell* **23**: 4476–4491.

Dobáková M, Sobotka R, Tichý M, Komenda J. 2009. Psb28 protein is involved in the biogenesis of the photosystem II inner antenna CP47 (PsbB) in the cyanobacterium *Synechocystis* sp. PCC 6803. *Plant Physiology* **149**: 1076–1086.

Ermakova-Gerdes S, Vermaas WFJ. 1999. Inactivation of the open reading frame *slr0399* in *Synechocystis* sp. PCC 6803 functionally complements mutations near the Q(A) niche of photosystem II. A possible role of Slr0399 as a chaperone for quinone binding. *Journal of Biological Chemistry* **274**: 30540–30549.

Fang Y, Zhao S, Zhang F, Zhao A, Zhang W, Zhang M, Liu L. 2016. The Arabidopsis glutamyl-tRNA reductase (GluTR) forms a ternary complex with FLU and GluTR-binding protein. *Scientific Reports* **6**: 19756.

Flores E, Arévalo S, Burnat M. 2019. Cyanophycin and arginine metabolism in cyanobacteria. *Algal Research* **42**: 101577.

de la Fuente A, Martin JF, Rodriguez-Garcia A, Liras P. 2004. Two proteins with ornithine acetyltransferase activity show different functions in *Streptomyces clavuligerus*: Oat2 modulates clavulanic acid biosynthesis in response to arginine. *Journal of Bacteriology* **186**: 6501–6507.

Hanaichi T, Sato T, Iwamoto T, Malavasi-Yamashiro J, Hoshino M, Mizuno N. 1986. A stable lead by modification of Sato's method. *Journal of Electron Microscopy* **35**: 304–306.

Heinz S, Liauw P, Nickelsen J, Nowaczyk M. 2016. Analysis of photosystem II biogenesis in cyanobacteria. *Biochimica et Biophysica Acta-Bioenergetics* **1857**: 274–287.

Herranen M, Battchikova N, Zhang PP, Graf A, Sirpio S, Paakkarinen V, Aro EM. 2004. Towards functional proteomics of membrane protein complexes in *Synechocystis* sp PCC 6803. *Plant Physiology* **134**: 470–481.

Hollingshead S, Kopečná J, Jackson PJ, Canniffe DP, Davison PA, Dickman MJ, Sobotka R, Hunter CN. 2012. Conserved chloroplast open-reading frame

ycf54 is required for activity of the magnesium protoporphyrin monomethylester oxidative cyclase in *Synechocystis* PCC 6803. *Journal of Biological Chemistry* **287**: 27823–27833.

Hou Z, Pang X, Hedtke B, Grimm B. 2021. *In vivo* functional analysis of the structural domains of FLUORESCENT (FLU). *The Plant Journal* **107**: 360–376.

Hou Z, Yang Y, Hedtke B, Grimm B. 2019. Fluorescence in blue light (FLU) is involved in inactivation and localization of glutamyl-tRNA reductase during light exposure. *The Plant Journal* **97**: 517–529.

Katoh K, Standley DM. 2013. MAFFT multiple sequence alignment software version 7: improvements in performance and usability. *Molecular Biology and Evolution* **30**: 772–780.

Keseler IM, Collado-Vides J, Gama-Castro S, Ingraham J, Paley S, Paulsen IT, Peralta-Gil M, Karp PD. 2005. EcoCyc: a comprehensive database resource for *Escherichia coli*. *Nucleic Acids Research* **33**(Database issue): D334–D337.

Knoppová J, Sobotka R, Tichý M, Yu J, Koník P, Halada P, Nixon PJ, Komenda J. 2014. Discovery of a chlorophyll binding protein complex involved in the early steps of photosystem II assembly in *Synechocystis*. *Plant Cell* **26**: 1200–1212.

Komenda J, Sobotka R. 2019. Chlorophyll-binding subunits of photosystem I and II: Biosynthesis, chlorophyll incorporation and assembly. In: Grimm B, ed. *Metabolism, structure and function of plant tetrapyrroles: Control mechanisms of chlorophyll biosynthesis and analysis of chlorophyll-binding proteins*. Amsterdam, the Netherlands: Elsevier, 195–223.

Kopečná J, Pilný J, Krynická V, Tomčala A, Kis M, Gombos Z, Komenda J, Sobotka R. 2015. Lack of phosphatidylglycerol inhibits chlorophyll biosynthesis at multiple sites and limits chlorophyllide reutilization in the cyanobacterium *Synechocystis* 6803. *Plant Physiology* **169**: 1307–1317.

Kopf M, Klähn S, Scholz I, Matthiessen JKF, Hess WR, Voß B. 2014. Comparative analysis of the primary transcriptome of *Synechocystis* sp. PCC 6803. *DNA Research* **21**: 527–539.

Koskela MM, Skotnicová P, Kiss É, Sobotka R. 2020. Purification of protein-complexes from the cyanobacterium *Synechocystis* sp. PCC 6803 using FLAG-affinity chromatography. *Bio-Protocol* **10**: e3616.

Lee J, Lee HJ, Shin MK, Ryu WS. 2004. Versatile PCR-mediated insertion or deletion mutagenesis. *BioTechniques* **36**: 398–400.

Livak KJ, Schmittgen TD. 2001. Analysis of relative gene expression data using real-time quantitative PCR and the 2(-Delta Delta C(T)) Method. *Methods* **25**: 402–408.

Marc F, Weigel P, Legrain C, Glansdorff N, Sakanyan V. 2001. An invariant threonine is involved in self-catalyzed cleavage of the precursor protein for ornithine acetyltransferase. *Journal of Biological Chemistry* **276**: 25404–25410.

Mareš J, Strunecký O, Bučinská L, Wiedermannová J. 2019. Evolutionary patterns of thylakoid architecture in cyanobacteria. *Frontiers in Microbiology* **10**: 277.

Morimoto K, Nishio K, Nakai M. 2002. Identification of a novel prokaryotic HEAT-repeats-containing protein which interacts with a cyanobacterial IscA homolog. *FEBS Letters* **519**(1–3): 123–127.

Morimoto K, Sato S, Tabata S, Nakai M. 2003. A HEAT-repeats containing protein, IaiH, stabilizes the iron-sulfur cluster bound to the cyanobacterial IscA homologue, IscA2. *Journal of Biochemistry* **134**: 211–217.

Nagano N, Hutchinson EG, Thornton JM. 1999. Barrel structures in proteins: automatic identification and classification including a sequence analysis of TIM barrels. *Protein Science* **8**: 2072–2084.

Nellaepalli S, Ozawa S-I, Kuroda H, Takahashi Y. 2018. The photosystem I assembly apparatus consisting of Ycf3–Y3IP1 and Ycf4 modules. *Nature Communications* **9**: 2439.

Phillips JD, Bergonia HA, Reilly CA, Franklin MR, Kushner JP. 2007. A porphomethene inhibitor of uroporphyrinogen decarboxylase causes porphyria cutanea tarda. *Proceedings of the National Academy of Sciences, USA* **104**: 5079–5084.

Pilný J, Kopečná J, Noda J, Sobotka R. 2015. Detection and quantification of heme and chlorophyll precursors using a High Performance Liquid Chromatography (HPLC) system equipped with two fluorescence detectors. *Bio-Protocol* **5**: e1390.

Pinto FL, Thapper A, Sontheim W, Lindblad P. 2009. Analysis of current and alternative phenol based RNA extraction methodologies for cyanobacteria. *BMC Molecular Biology* **10**: 79.

Richter AS, Banse C, Grimm B. 2019. The GluTR-binding protein is the heme-binding factor for feedback control of glutamyl-tRNA reductase. *eLife* **13**: e46300.

Roose JL, Frankel LK, Bricker TM. 2014. The PsbP domain protein 1 functions in the assembly of lumenal domains in photosystem I. *Journal of Biological Chemistry* **289**: 23776–23785.

Schwabe TM, Gloddek K, Schluesener D, Kruip J. 2003. Purification of recombinant BtpA and Ycf3, proteins involved in membrane protein biogenesis in *Synechocystis* PCC 6803. *Journal of Chromatography. B, Analytical Technologies in the Biomedical and Life Sciences* **786**: 45–59.

Shen J, Williams-Carrier R, Barkan A. 2017. PSA3, a potein on the sromal fce of the thylakoid membrane, promotes Photosystem I accumulation in cooperation with the assembly factor PYG7. *Plant Physiology* **174**: 1850–1862.

Skotnicová P, Staleva-Musto H, Kuznetsova V, Bína D, Konert MM, Lu S, Polívka T, Sobotka R. 2021. Plant LHC-like proteins show robust folding and static non-photochemical quenching. *Nature Communications* **12**: 6890.

Sobotka R, Komenda J, Bumba L, Tichý M. 2005. Photosystem II assembly in CP47 mutant of *Synechocystis* sp PCC 6803 is dependent on the level of chlorophyll precursors regulated by ferrochelatase. *Journal of Biological Chemistry* **280**: 31595–31602.

Sobotka R, McLean S, Žuberová M, Hunter CN, Tichý M. 2008. The C-terminal extension of ferrochelatase is critical for enzyme activity and for functioning of the tetrapyrrole pathway in *Synechocystis* strain PCC 6803. *Journal of Bacteriology* **190**: 2086–2095.

Tichý M, Bečková M, Kopečná J, Noda J, Sobotka R, Komenda J. 2016. Strain of *Synechocystis* PCC 6803 with aberrant assembly of photosystem II contains tandem duplication of a large chromosomal region. *Frontiers in Plant Science* **7**: 648.

Vavilin D, Brune DC, Vermaas W. 2005. N-15-labeling to detennine chlorophyll synthesis and degradation in *Synechocystis* sp PCC 6803 strains lacking one or both photosystems. *Biochimica et Biophysica Acta-Bioenergetics* **1708**: 91–101.

Wang P, Grimm B. 2021. Connecting chlorophyll metabolism with accumulation of the photosynthetic apparatus. *Trends in Plant Science* **26**: 484–495.

Zak E, Norling B, Andersson B, Pakrasi HB. 1999. Subcellular localization of the BtpA protein in the cyanobacterium *Synechocystis* sp. PCC 6803. *European Journal of Biochemistry* **261**: 311–316.

Zak E, Pakrasi HB. 2000. The BtpA protein stabilizes the reaction center proteins of photosystem I in the cyanobacterium *Synechocystis* sp PCC 6803 at low temperature. *Plant Physiology* **123**: 215–222.

Zhao A, Fang Y, Chen X, Zhao S, Dong W, Lin Y, Gong W, Liu L. 2014. Crystal structure of Arabidopsis glutamyl-tRNA reductase in complex with its stimulator protein. *Proceedings of the National Academy of Sciences, USA* **111**: 6630–6635.

Supporting Information

Additional Supporting Information may be found online in the Supporting Information section at the end of the article.

Fig. S1 Photoautotrophic growth of several mutated strains on agar plates and formation of Δ*btpA* revertants.

Fig. S2 Ultrastructure of WT and Δ*btpA* cells analyzed by transmission electron microscopy.

Fig. S3 Structural model of the homodimeric *Synechocystis* GluTR enzyme.

Fig. S4 Colocalization of BtpA and GluTR in soluble fraction and co-isolation of GluTR with f.BtpA.

Fig. S5 Absorption spectra of unknown uroporphyrin-like pigments accumulated in the *btpA*-s2 strain.

Fig. S6 Mapping the identified tryptic MS peptides on the sequence of *Synechocystis* ArgJ.

Fig. S7 Predicted structure of BtpA and SgcQ proteins and conserved residues.

Fig. S8 Level of PP$_{IX}$ in the *sgcQ* null mutant of *E. coli*.

Methods S1 Quantitative LC–MS/MS analysis of 5-ALA.

Methods S2 Protein mass spectrometry.

Methods S3 Electron microscopy.

Table S1 List of *Synechocystis* mutant strains described in this study.

Table S2 List of primers used to prepare *Synechocystis* mutant strains.

Table S3 Multiple reaction monitoring transitions used for the LC–MS/MS quantification of 5-ALA.

Table S4 Identification of protein bands detected on a Coomassie blue stained SDS-PAGE of the separated f.BtpA and f.GluTR elutions.

Please note: Wiley is not responsible for the content or functionality of any Supporting Information supplied by the authors. Any queries (other than missing material) should be directed to the *New Phytologist* Central Office.